Task Title A Finite Element Conjugate Gradient FFT Method for Scattering

Investigators J.D. Collins, Dan Ross, J.M.-Jin, A. Chatterjee and J.L. Volakis

Period Covered Sept. 1990 - Feb. 1991

ABSTRACT

Validated results are presented for the new 3D body of revolution finite element-boundary integral code. As usual, a Fourier Series expansion of the vector electric and magnetic fields is employed to reduce the dimensionality of the system and the exact boundary condition is employed to terminate the finite element mesh. The mesh termination boundary is chosen such that it leads to convolutional boundary operators for low O(n) memory demand. Improvements of this code are discussed along with the proposed formulation for a full 3D implementation of the finite element-boundary integral method in conjunction with a CGFFT solution.

OBJECTIVE

The objective of this task is to develop innovative techniques and related software for scattering by three dimensional composite structures. The proposed analysis is a hybrid finite element-boundary integral method formulated to have an O(n) memory demand. This low storage is achieved by employing the FFT to evaluate all boundary integrals and by resorting to an iterative solution algorithm. Particular emphasis in this task is the generation of software applicable to airborne vehicles and the validation of these by comparison with measured and other reference data. Because the approach is new, a step by step development procedure has been proposed over a three-year period. During the first year the technique was developed and implemented for two-dimensional composite structures. Support software for the two-dimensional analysis such as pre- and post-processor routines were developed during the second year and a formulation was also developed and implemented for three-dimensional bodies of revolution. Finally, during the third year, we will develop, implement, and test the method for arbitrary three dimensional structures.

BACKGROUND

Interest in three-dimensional (3-D) methods has increased in recent years, however, the associated demands in computation time and storage are often prohibitive for electrically large 3-D bodies. Vector and concurrent (i.e. hypercube, connection, etc.) computers are beginning to alleviate the first of these demands, but a minimization of the storage requirements is essential for treating large structures.

The traditional Conjugate Gradient Fast Fourier Transform (CGFFT) method [1] - [4] is one such frequency domain solution approach which requires O(n) storage for the solution on n equations. This method involves the use of FFTs whose dimension equals that of the structure under consideration [5] - [7] and, therefore, demands excessive computation time when used in an iterative algorithm. Also, the standard CGFFT requires uniform rectangular gridding that unnecessarily includes the impenetrable portions of the scatterer. With these issues in mind, a new solution approach is proposed for solving scattering problems. The proposed method will be referred to as the Finite Element-Conjugate Gradient Fast Fourier Transform (FE-CGFFT) method.

During last year's effort the FE-CGFFT method was developed for two-dimensional scatterers where the finite element mesh was terminated at a rectangular box. Inside the box boundaries, Helmholtz equation is solved via the finite element method and the boundary constraint is obtained by an appropriate integral equation which implicitly satisfies the radiation condition. Along the parallel sides of the box, this integral becomes a convolution and is, therefore, amenable to evaluation via the FFT. The dimension of the required FFT in this hybrid method is one less than the dimensionality of the structure thus, making it attractive for 3-D simulations. Also, because it incorporates the finite element method, the FE-CGFFT formulation remains valid regardless of the structure's geometry and material composition.

The proposed method described in the University of Michigan Report 025921-6-T (see also [8]) is similar to the moment method version developed by Jin [9]. Jin's method was in turn based on work published in the early 70's by McDonald and Wexler [10] who introduced an approach to solve unbounded field problems. The proposed method is also similar to other methods (a few of which will be mentioned here), neither of which provides a storage reduction comparable to the proposed FE-CGFFT method. The unimoment method [11] uses finite elements inside a fictitious circular boundary and an eigenfunction expansion to represent the field in the external region. The coefficients of the expansion are then determined by enforcing field continuity at the finite element (FE) mesh boundary. The coupled finite element-boundary element method [12] uses the finite element method within the boundary and the boundary element method to provide the

additional constraint at the termination of the mesh. Unlike the proposed method, the solution in [12] was accomplished by direct matrix inversion (as in [9]), and the outer mesh boundary is not rectangular to take advantage of the FFT for the evaluation of the boundary integrals.

PROGRESS

Part of our efforts in this task were devoted to debugging and validating the three dimensional body of revolution (BOR) code developed in the previous months. The analysis associated with this code is described in the U of M technical report 025921-18-T where we also include validation data obtained over the past two months. Some of these are shown in figures 1-3 and refer to an ogive, a circular cylinder and a sphere. Unfortunately, it was found that as the bodies became larger the system's condition deteriorates and this was traced to the pulse basis formulation employed for the discretization of the boundary. Through several tests we have now shown that A Galerkin's linear basis formulation will correct the convergence difficulties. For example, this formulation was already employed in solving large systems (with more than 120,000 unknowns) associated with the scattering by frequency selective surfaces (FSS) and large Mates. As shown in figure 4-5, the Galerkin's formulation with linear basis permitted a solution of this system in less than 70 iterations! In comparison, the pulse basis-point matching formulation would require several thousand iterations before reaching convergence. Consequently, we are in the process of incorporating the Galerkin's linear basis formulation into our existing 2D and 3D BOR codes. Further, it was found that the ech area converges much sooner than the mean square error and permitted us to speed-up solution time.

During this last quarter we also began the development of the proposed finite element formulation for general non-symmetric inhomogeneous bodies. The basic discrete elements in this case are tetrahedra in conjunction with edge-based expansion functions. The associated finite element formulations is described in Appendix A and we are now in the process of implementing it. Initially, the finite element mesh will be terminated by a fictitious absorbing layer whose dielectric parameters were determined by a minimization of the reflection coefficient over the entire range of incidence angles. For a three layer coating, each of thickness 0.05 wavelengths, it was found that their respective dielectric properties to minimize the reflection coefficient over all angles of incidence are

ε_{r1}=(-0.1249205, -1.731605), μ_{r1}=(-1.031792, -0.1039932)
ε_{r2}=(0.040699530, 0.1750280), μ_{r1}=(0.3155941, 0.3190330)
ε_{r3}=(-1.278644, 0.9625375), μ_{r3}=(-0.1721315, -5.389832)

The corresponding plot of the reflection coefficient as a function of incidence is given in figure 7 along with scattering patterns based on the proposed termination model. As seen, for the chosen fictitious absorber the reflection coefficient is less than one percent for θ up to 62 degrees and less than 2 percent for θ up to 77 degrees. For the same error criteria, the corresponding angles associated with the second order Padé ABC are 35 and 41 degrees, respectively. The fictitious ABC has, therefore, a substantially better performance over the existing ABCs, and its effectiveness will be examined further in the next few months.

The three dimensional finite element meshes required in the analysis will be generated by SDRC IDEAS and we have already began to develop the software for transforming the output of this commercial package to the input files of our analysis codes. Similar drivers were already developed for the two dimensional code which was developed last year.

Finally, during this period we performed extensive testing of the two-dimensional code and have in the progress developed several new pre- and post- processing algorithms for this code. Two of the new geometries (see fig. 8 and 11) whose scattering was computed with our 2D finite element - CGFFT code are displayed in figures 9, 11 and 12. These represent airfoil configurations, one of which is coated with a dielectric material.

CONCLUSIONS

The project continues to evolve in accordance with our original plan and schedule. Most importantly, so far, our expectation of the finite element CGFFT formulation have been realized and we are, therefore, pleased with its performance for the intended applications.

TRANSITIONS

All of our efforts in the next six months will be devoted to the development of the 3D finite element boundary integral code for arbitrary structures. In the immediate future we will also pursue improvements for our existing codes primarily directed at speeding the convergence of the CG or BiCG algorithm.

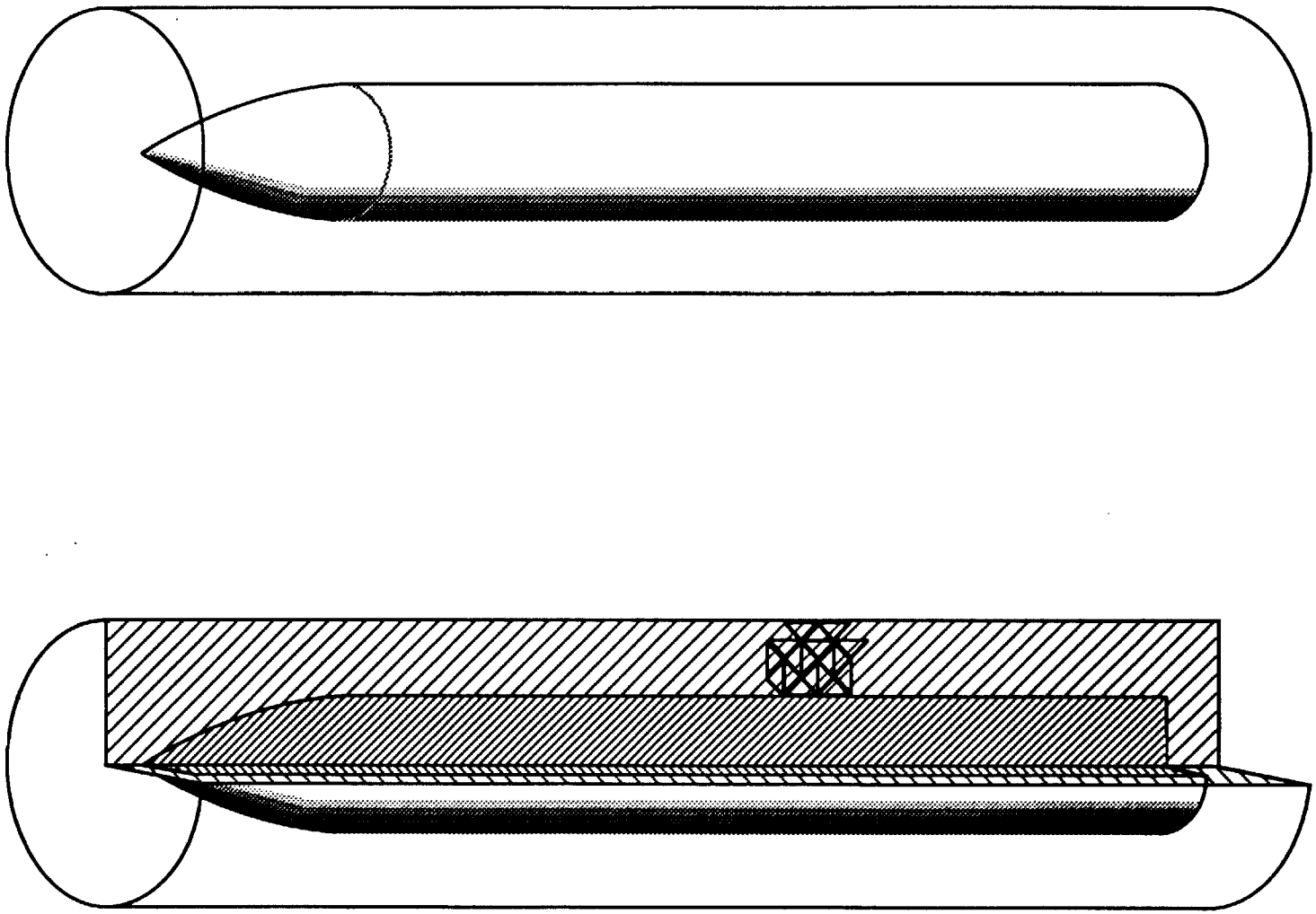

Body of Revolution enclosed in a fictitious finite length cylinder. Area between the Scatterer and the fictitious cylinder is discretized via the finite element method.

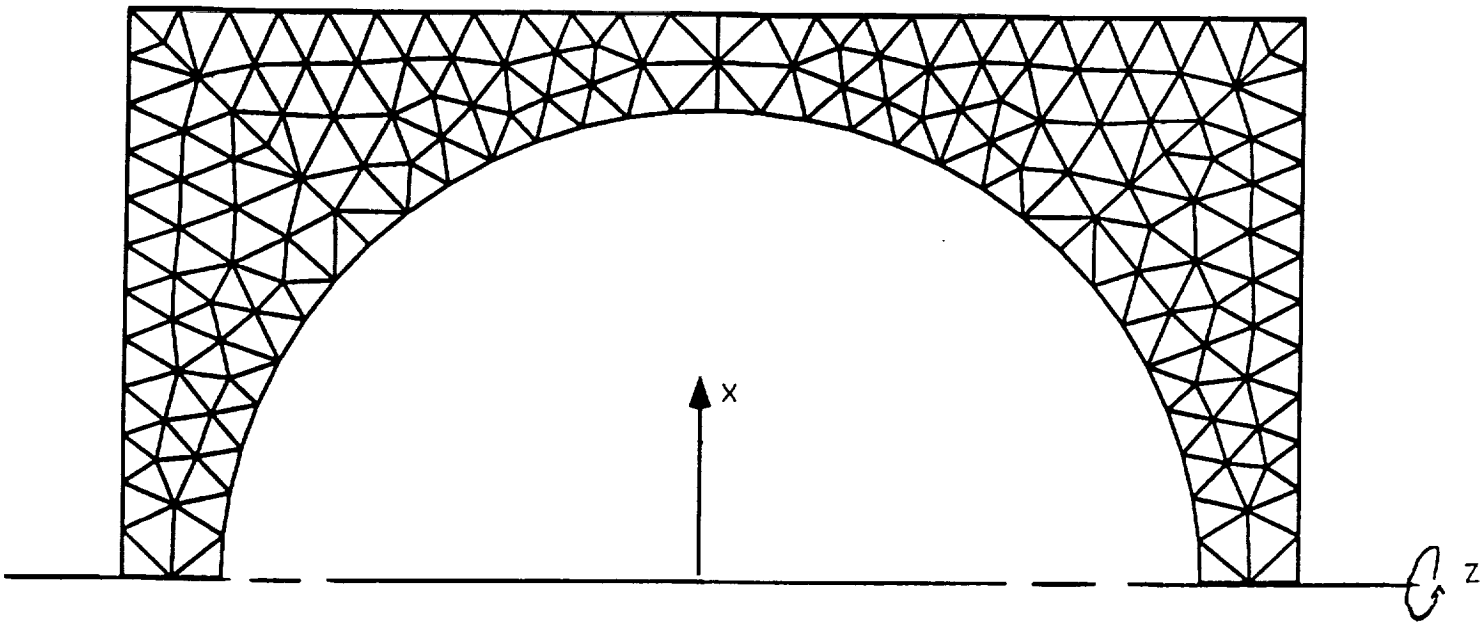

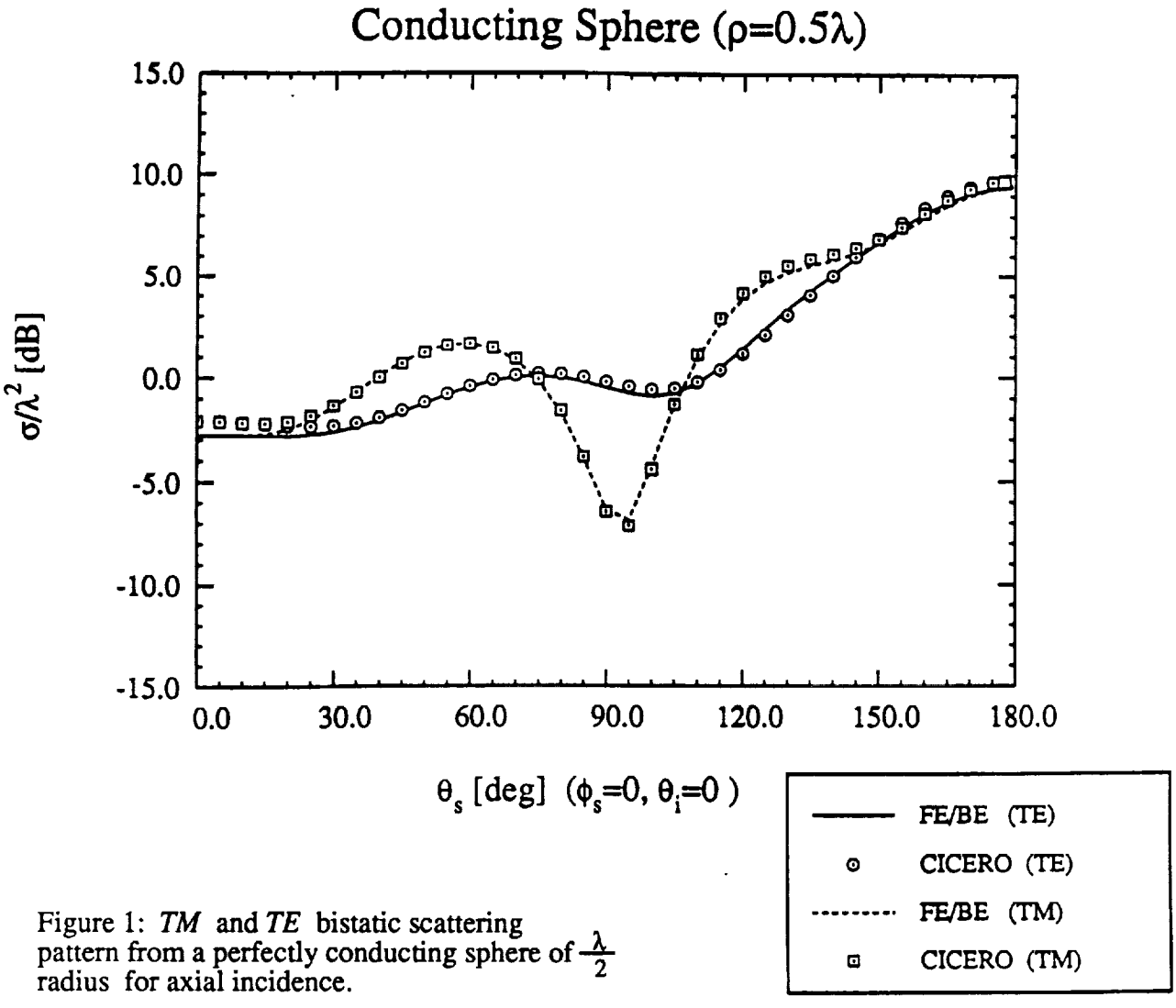

Figure 1: *TM* and *TE* bistatic scattering pattern from a perfectly conducting sphere of $\frac{\lambda}{2}$ radius for axial incidence.

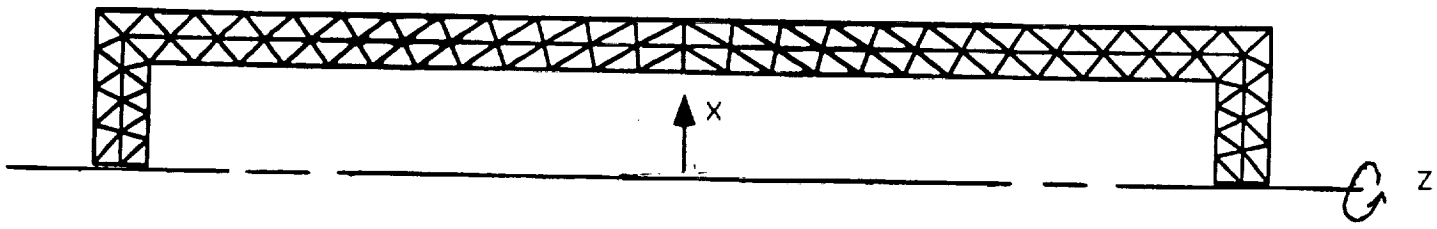

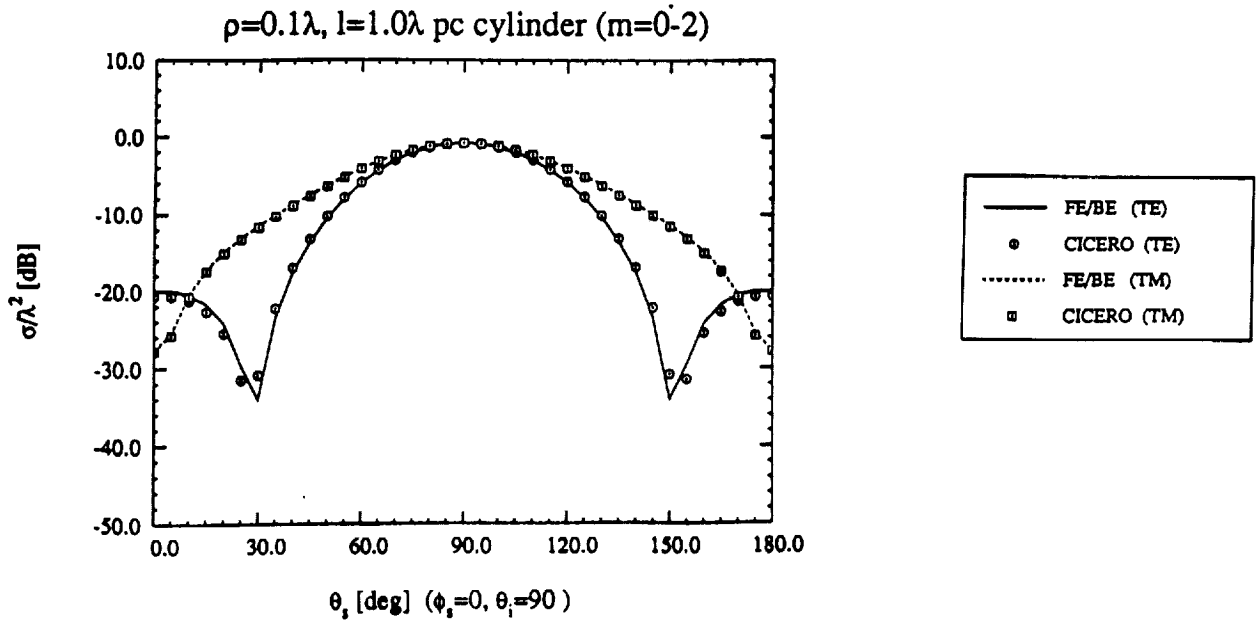

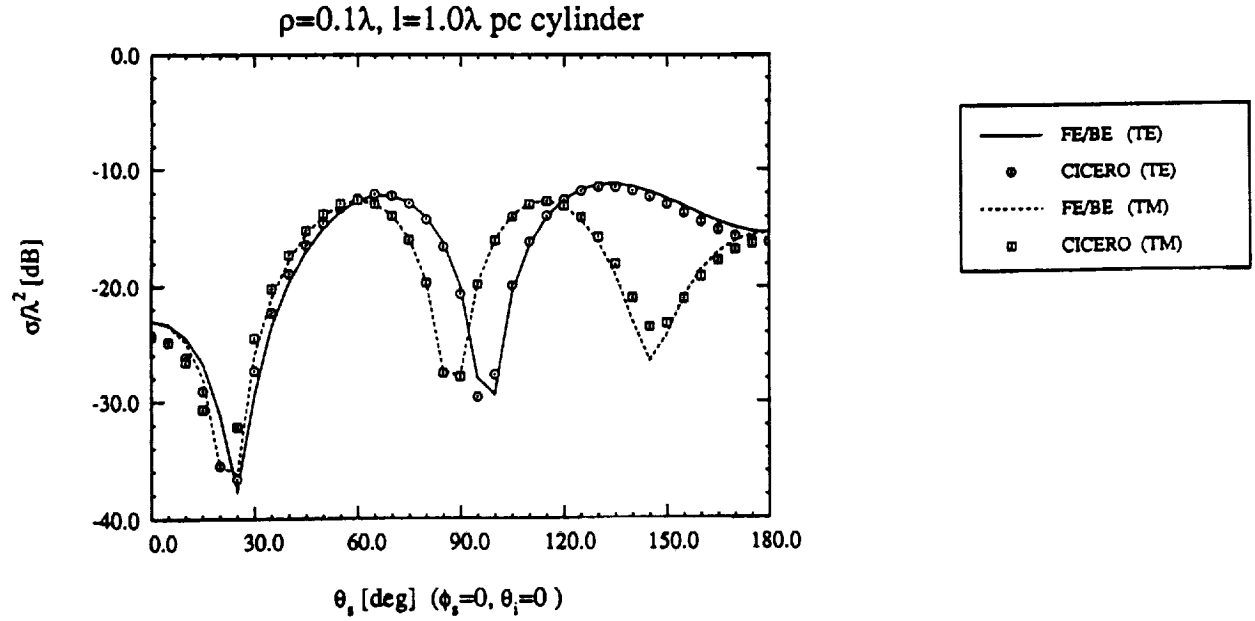

Figure 2: *TM* and *TE* bistatic scattering pattern from a perfectly conducting circular cylinder of length 1λ and radius 0.1λ for axial incidence. (a) modes 0-2, (b) converged

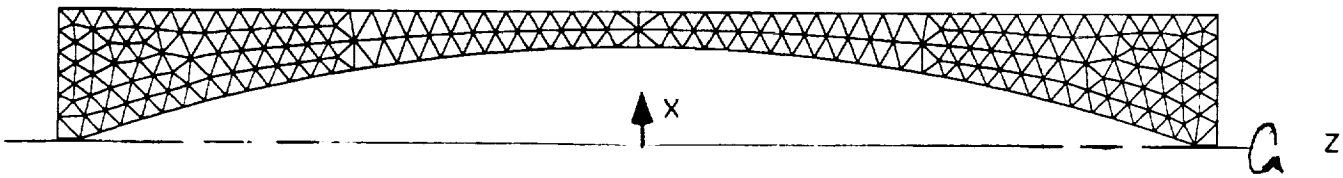

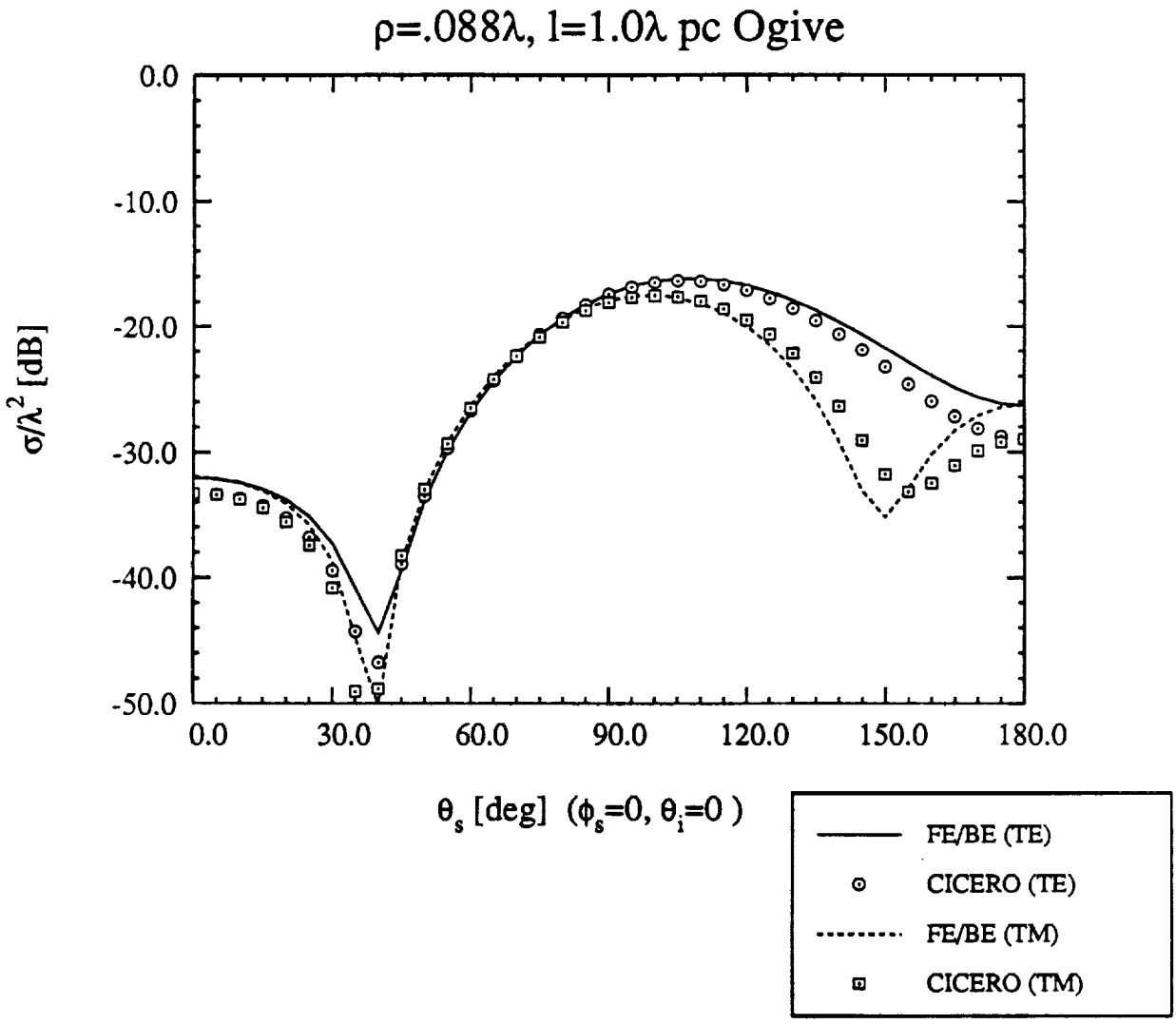

Figure 3: *TM* and *TE* bistatic scattering pattern from a perfectly conducting ogive length 1λ and maximum radius of 0.088λ for axial incidence.

12 x 12 FSS Array

f=24 GHz

$\phi^{inc} = 45^o$ $\theta^{inc} = 75^o$

28,084 Unknowns

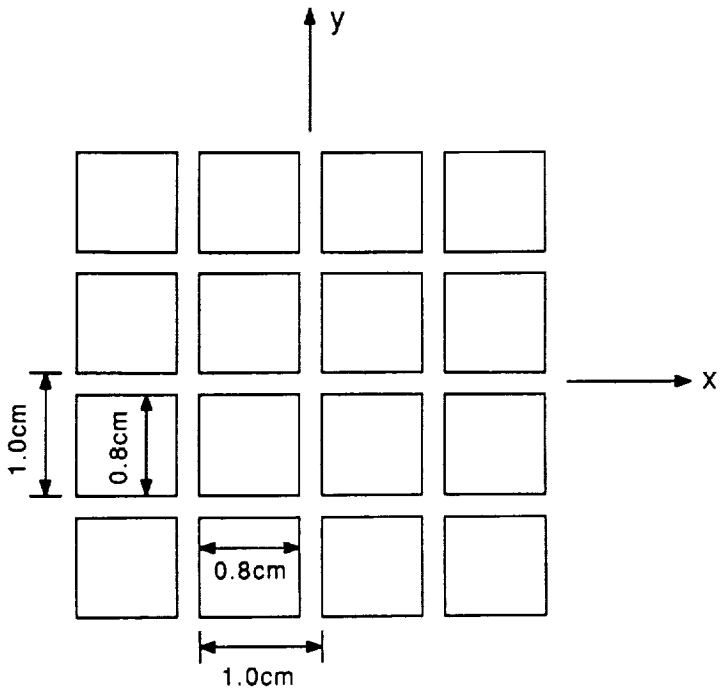

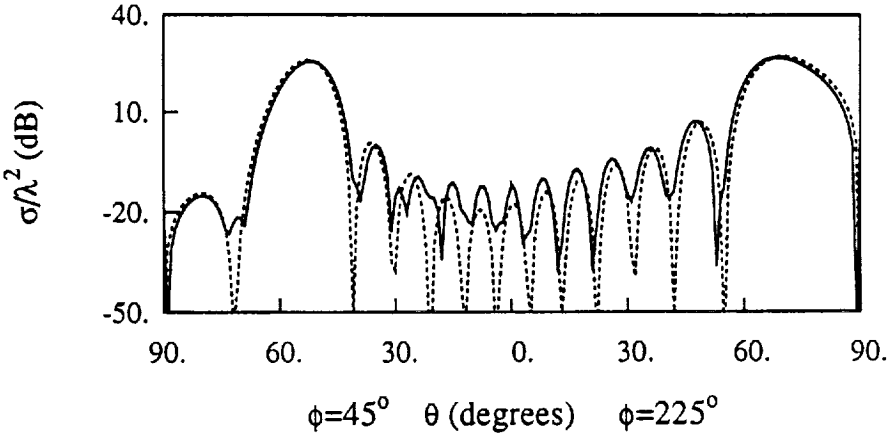

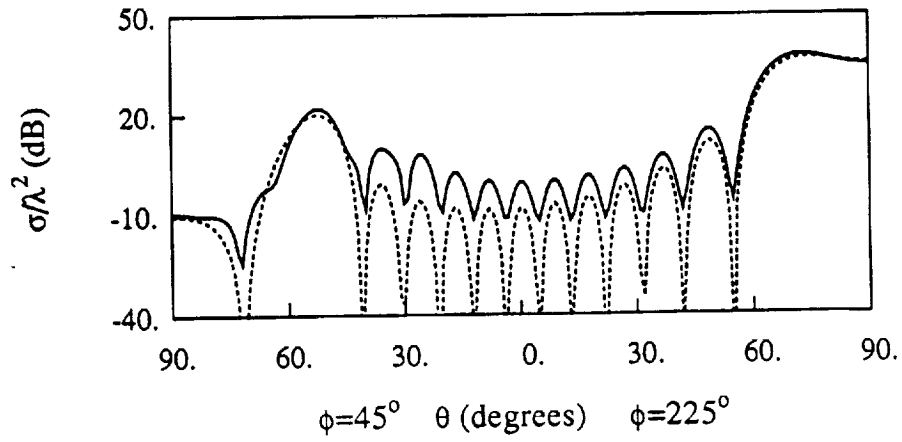

Figure 4: Scattering by a 12 x 12 FSS array; comparison of the exact solution (solid line) with an approximate result obtained by truncating the infinite FSS.

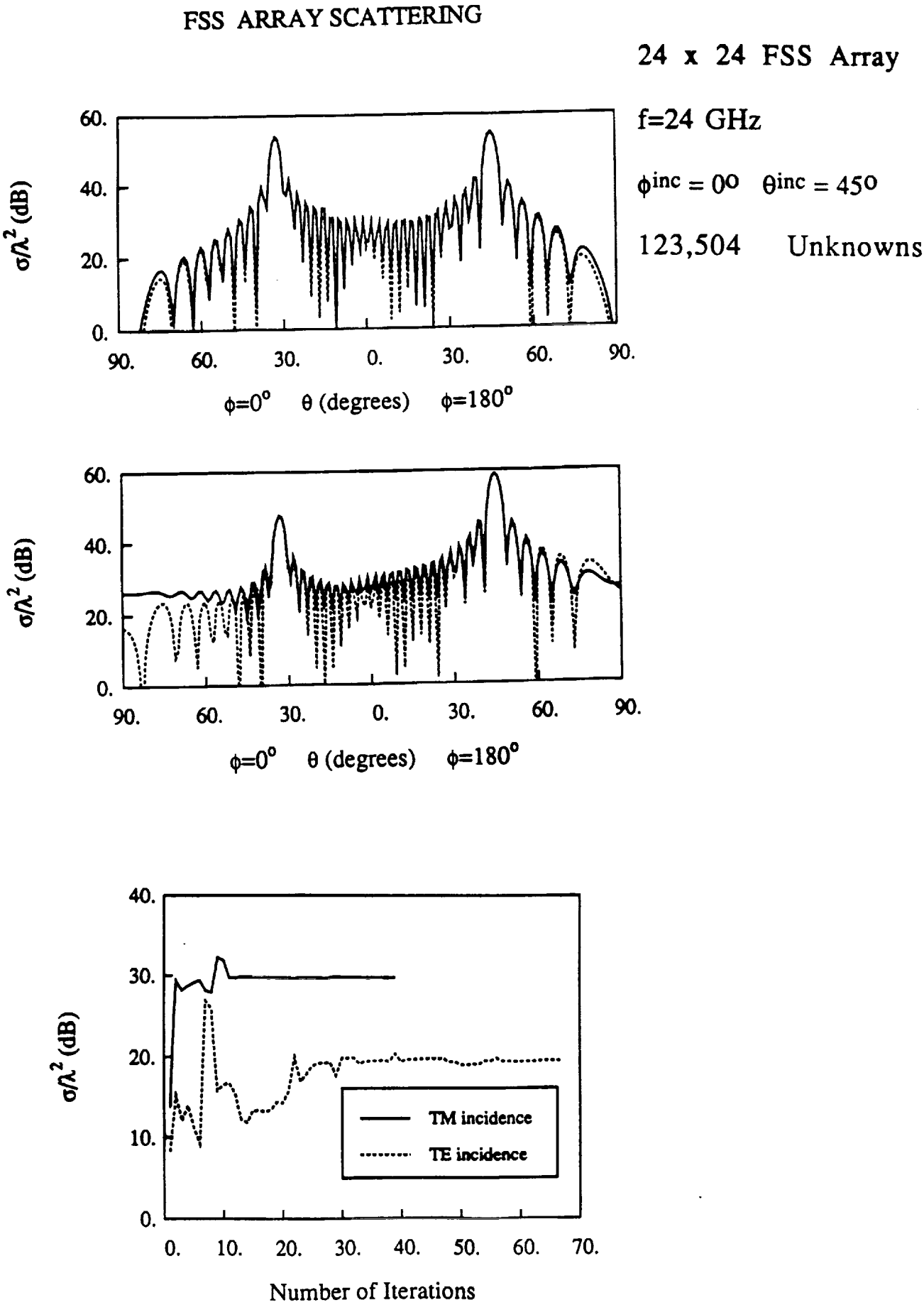

Figure 5: Scattering by a 24 x 24 array; comparison of the exact solution (solid line) with an approximate result obtained by truncating the infinite FSS.

Principal Plane Cut

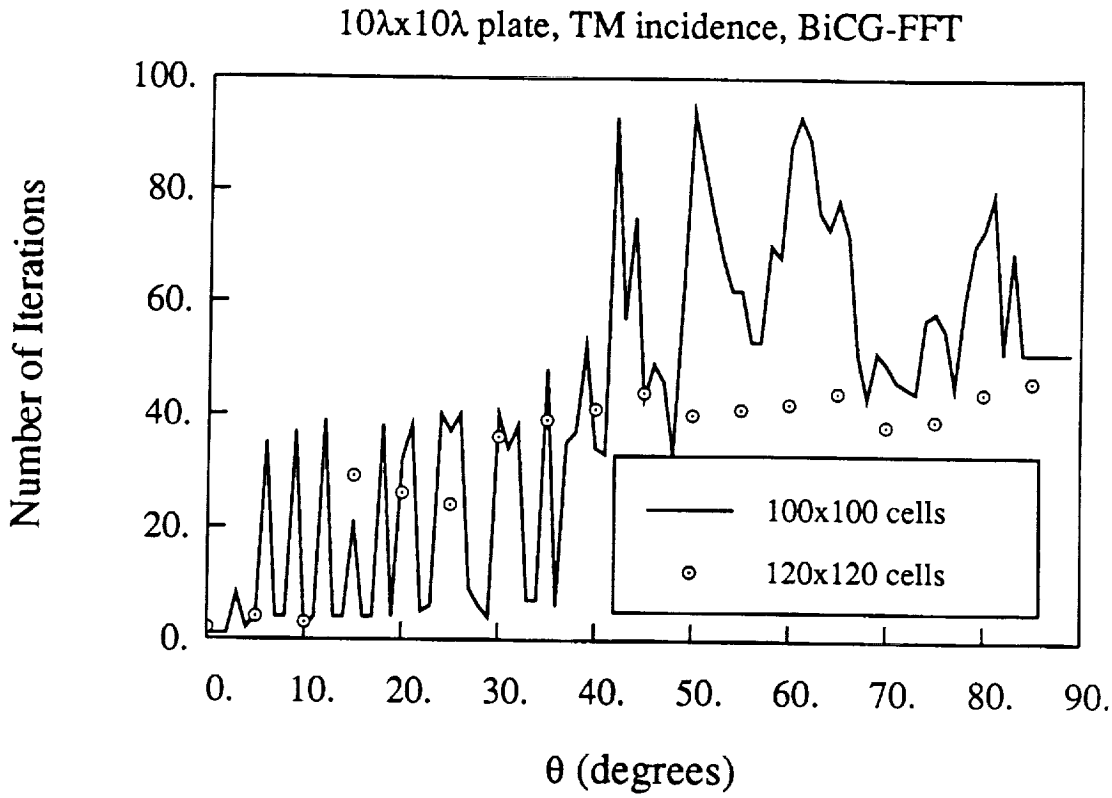

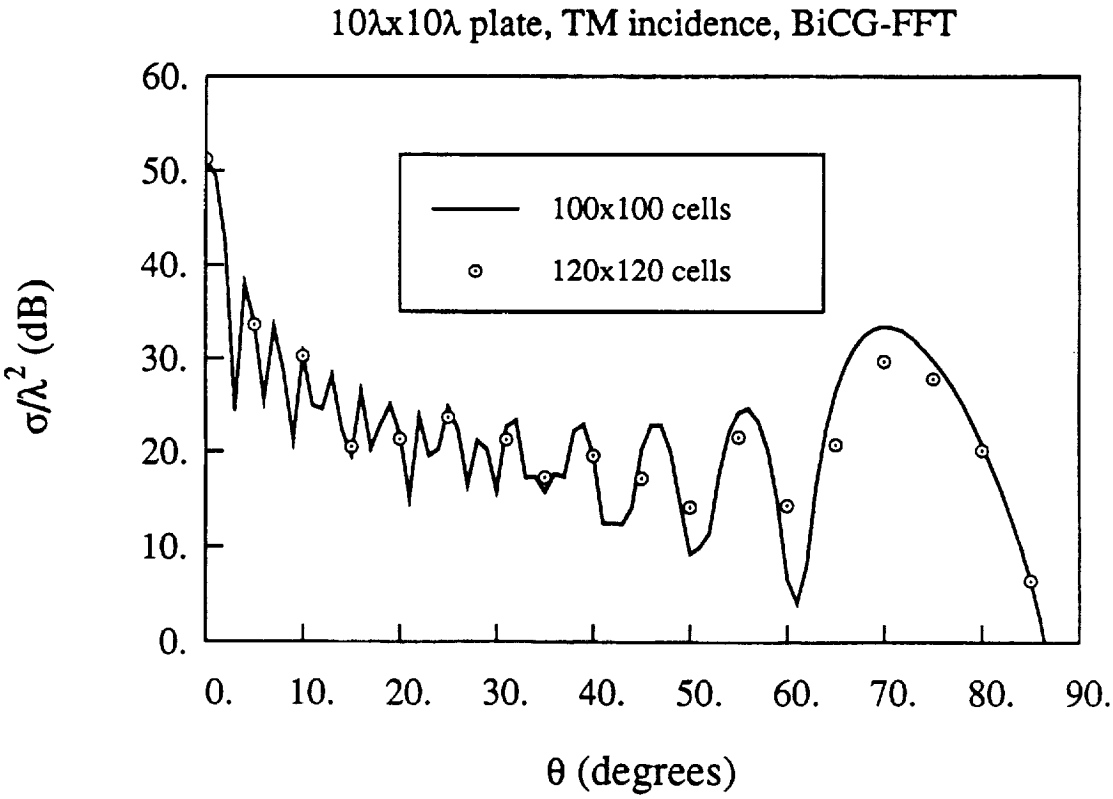

Figure 6: Principal plane *TM* Scattering by a 10λ x 10λ rectangular plate.

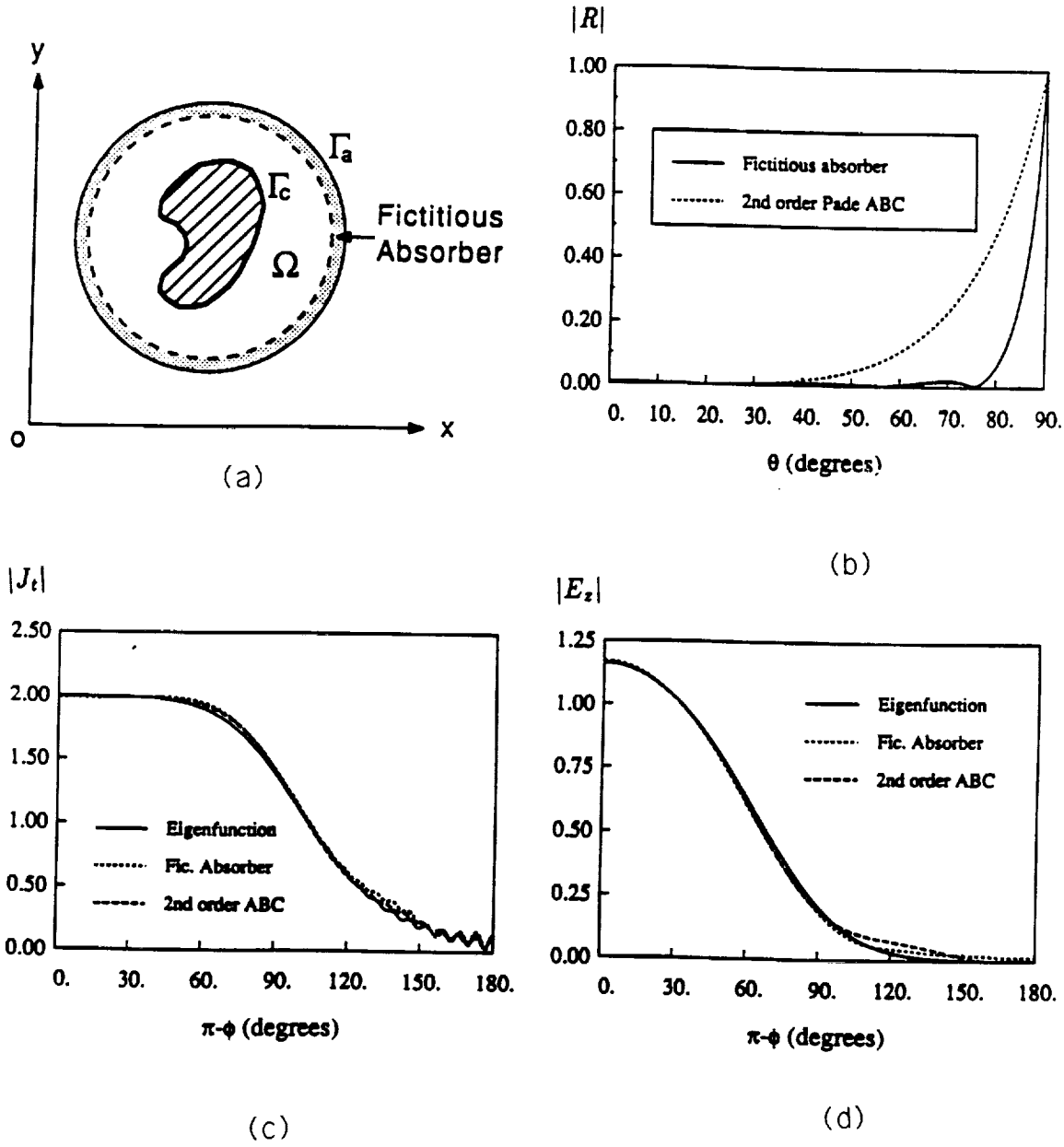

Figure 7: Evaluation of the new fictitious ABC (a) geometry (b) reflection coefficient plot (c) H_z field on a PEC Circular Cylinder (d) E_z field at a distance $\lambda/10$ from the surface of a PEC Circular Cylinder.

case 2: Coated Trailing Edge

$$y_{in} = \begin{cases} \pm\frac{1}{2}\sqrt{1-(x/2.5)^2} & -2.5 \le x \le 0 \\ \pm 0.8232\ A(x) & 0 \le x \le 2.5 \end{cases}$$

$$A(x) = \sqrt{\left(1-(x/2.7182)^2\right)} - 0.3926$$

$$y_{out} = \pm 0.8116\ B(x) \qquad 0.1 \le x \le 3.0$$

$$y_{out} = y_{in} \qquad \text{elsewhere}$$

$$B(x) = \sqrt{1-[(x-.1)/3.1416]^2} - .3846$$

$\varepsilon_r = 2 - j1$ between y_{in} and y_{out}

FEM Mesh

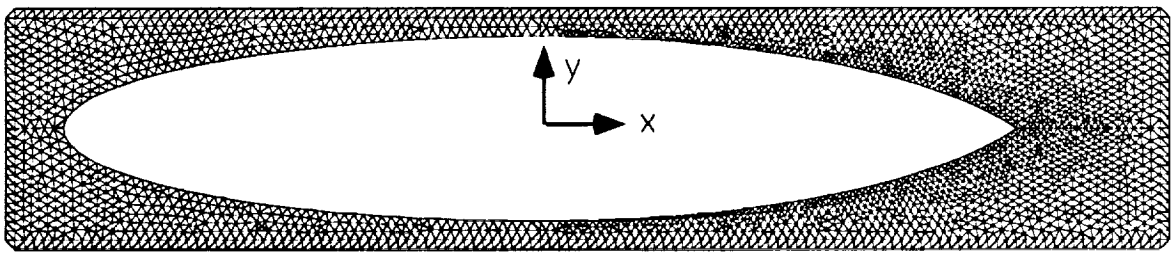

Figure 8: Geometry and finite element mesh of the illustrated coated trailing edge

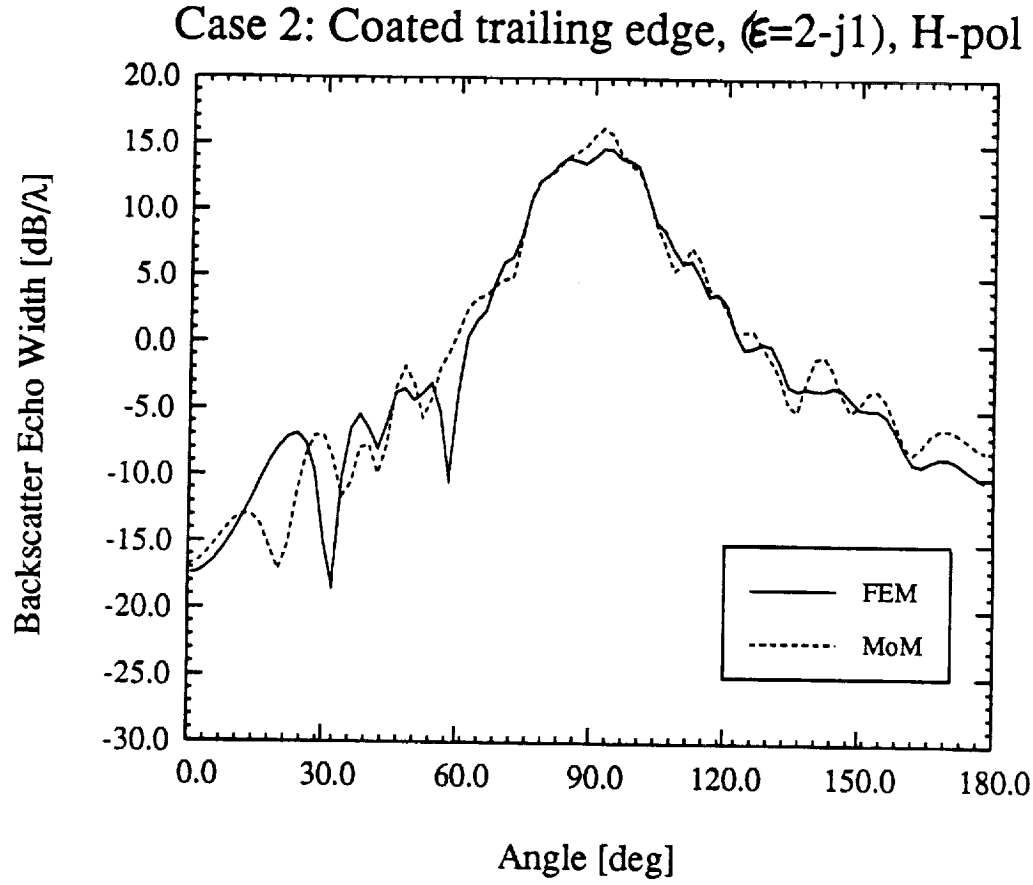

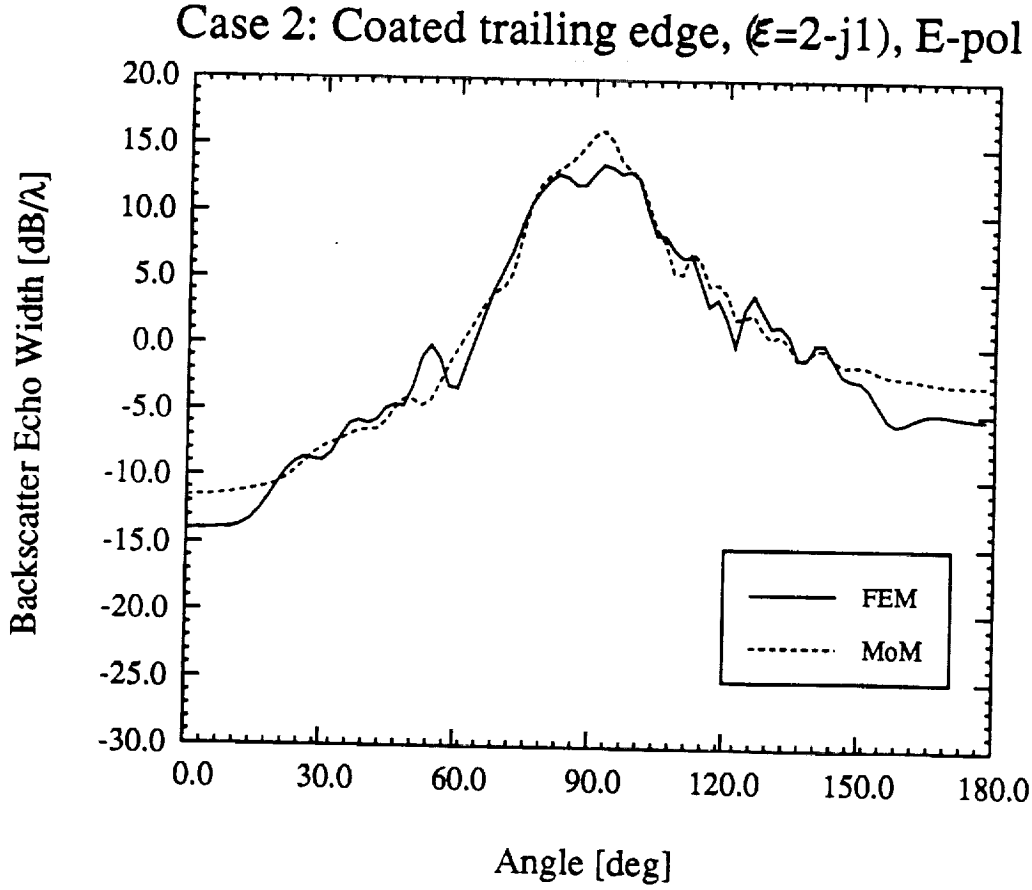

Figure 9: E and H polarization scattering patterns for the configuration shown in figure 8. Comparison of results between the FE-CGFFT and the moment method.

Perfectly conducting airfoil

All dimensions in wavelengths. The airfoil section is made by 5 arcs:

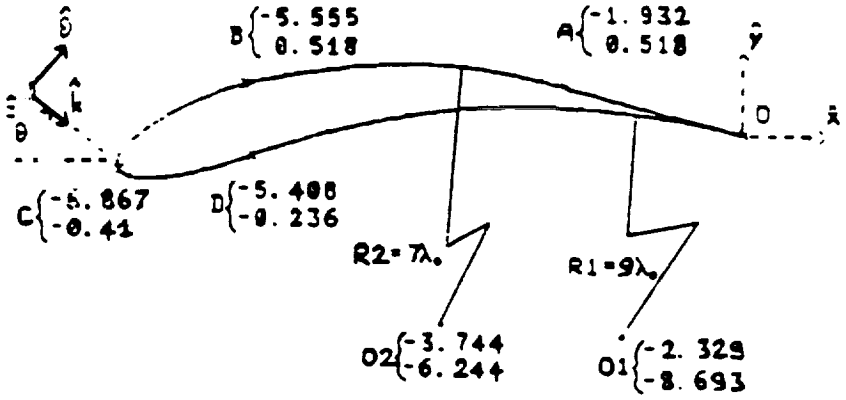

- **OA : straight line**
- **AB : circle of radius $R2 = 7\lambda_0$ and of center O2**
- **BC : polynomial parametric equation**
- **CD : polynomial parametric equation**
- **DO : circle of radius $R1 = 9\lambda_0$ and of center O1**

The polynomial equation are given by:

$$x(u) = \Sigma_{i=1}^{6} a_i \cdot u^{(6-i)} \quad y(u) = \Sigma_{i=1}^{6} b_i \cdot u^{(6-i)} \quad 0 \le u \le 1$$

a_i and b_i for BC arc				a_i and b_i for CD arc			
$a_1 =$	4.61149	$b_1 =$	1.53278	$a_1 =$	−1.62131	$b_1 =$	−0.12563
$a_2 =$	−12.11403	$b_2 =$	−3.22680	$a_2 =$	4.54389	$b_2 =$	0.30612
$a_3 =$	8.88606	$b_3 =$	0.90615	$a_3 =$	−3.32901	$b_3 =$	0.16113
$a_4 =$	0.44275	$b_4 =$	1.24623	$a_4 =$	0.35663	$b_4 =$	−0.00343
$a_5 =$	−0.51440	$b_5 =$	0.46927	$a_5 =$	−1.40984	$b_5 =$	−0.51216
$a_6 =$	−6.86720	$b_6 =$	−0.41007	$a_6 =$	−5.40756	$b_6 =$	−0.23609

Figure 10: Geometry of a PEC Airfoil whose scattering is given in figures 11 & 12.

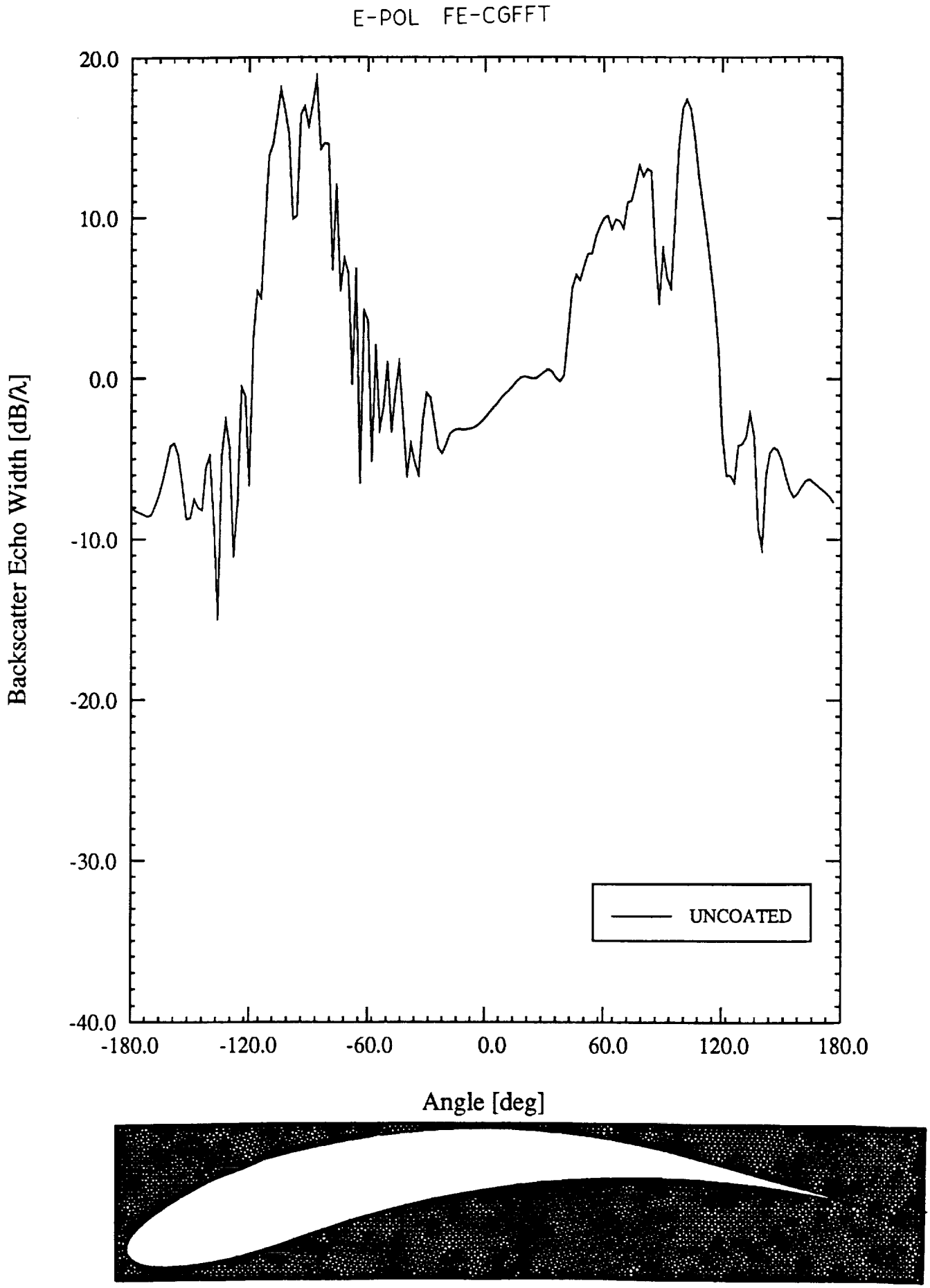

Figure 11: E-polarization echowidth for the airfoil given in figure 10.

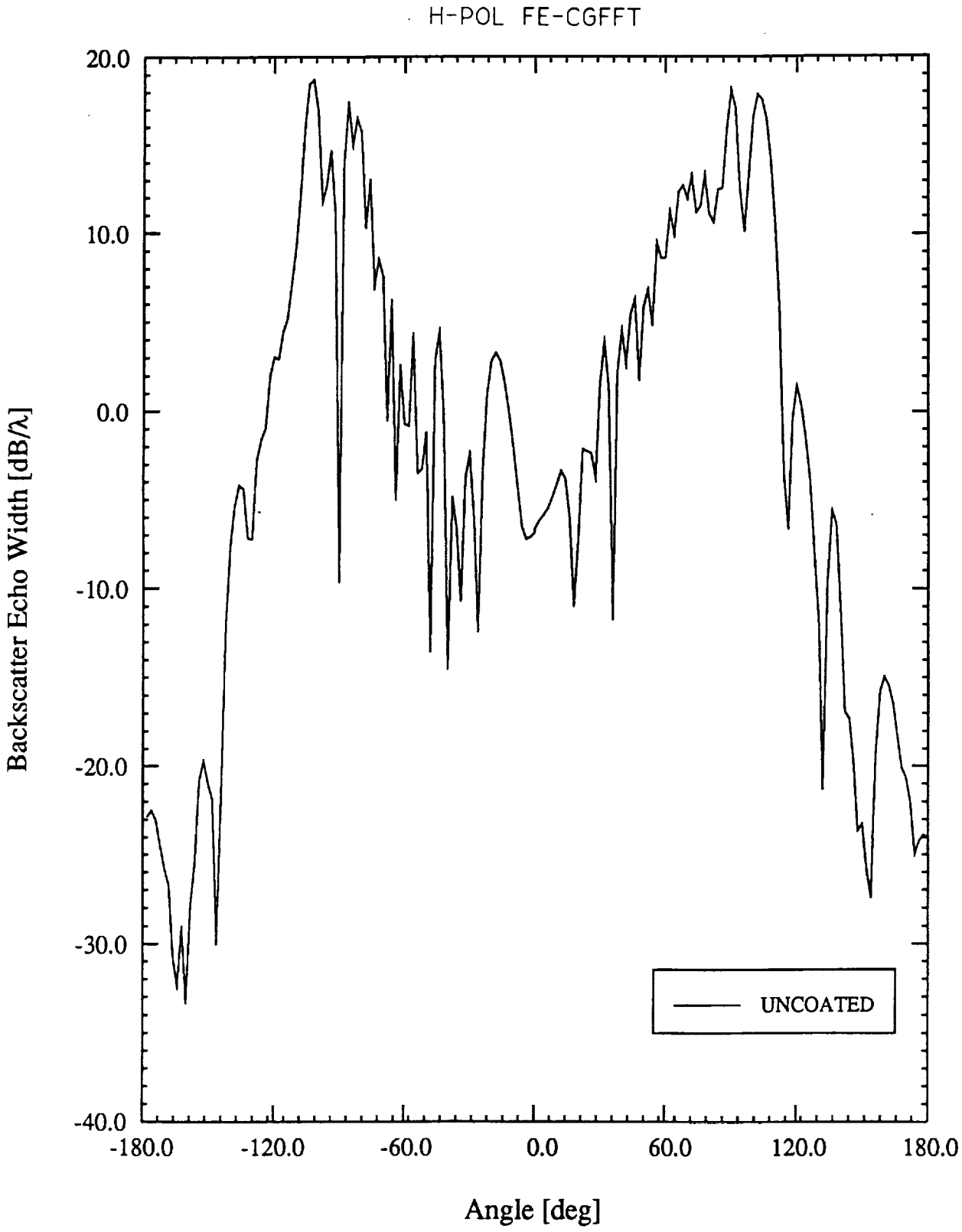

Figure 12: H-polarization echowidth for the airfoil given in figure 10.

Appendix A

Finite element formulation for tetrahedral elements and edge-based expansion basis

1 Derivation of finite element equations

Let us consider a three dimensional inhomogeneous body occupying the volume V. In order to discretize the electric field $\mathbf{E}$ inside the body, we subdivide the volume V into a number of small tetrahedra, each occupying volume $V_e(e = 1, 2, \cdots, M)$ with M being the total number of tetrahedral elements. Within each tetrahedron, the electric field satisfies the vector wave equation

$$\nabla \times \frac{1}{\mu_r} \nabla \times \mathbf{E} - k_o^2 \epsilon_r \mathbf{E} = \mathbf{0} \tag{1}$$

where μ_r is the permeability of the medium, ϵ_r is the medium permittivity and k_o is the free space wave number. The next step is to expand the electric field within V_e as

$$\mathbf{E} = \sum_{j=1}^{6} E_j^e \mathbf{W}_j^e \tag{2}$$

where $\mathbf{W}_j^e$ are edge-based vector basis functions and E_j^e denote the expansion coefficients of the basis, all defined within the volume V_e. $\mathbf{W}_j^e$ is tangential to the jth edge of the eth tetrahedron with zero tangential component along the other edges of the tetrahedral element. On substituting (2) into (1), we obtain

$$\sum_{j=1}^{6} E_j^e \left(\nabla \times \frac{1}{\mu_r} \nabla \times \mathbf{W}_j^e - k_o^2 \epsilon_r \mathbf{W}_j^e \right) = 0 \tag{3}$$

In order to solve for the unknown expansion coefficients E_j^e, we take the dot product of (3) with $\mathbf{W}_i^e$ and then integrate the resulting equation over the element volume V_e (Galerkin's technique). The wave equation thus reduces to

$$\sum_{j=1}^{6} E_j^e \int_{V_e} \mathbf{W}_i^e \cdot \left(\nabla \times \frac{1}{\mu_r} \nabla \times \mathbf{W}_j^e - k_o^2 \epsilon_r \mathbf{W}_j^e \right) dv = 0 \qquad (4)$$

The first term in the integral of the above expression can be simplified by using basic vector identities. Since

$$\mathbf{W}_i^e \cdot \left(\nabla \times \frac{1}{\mu_r} \nabla \times \mathbf{W}_j^e \right) = \nabla \cdot \left[\frac{1}{\mu_r} (\nabla \times \mathbf{W}_j^e) \times \mathbf{W}_i^e \right] + \frac{1}{\mu_r} (\nabla \times \mathbf{W}_i^e) \,.\, (\nabla \times \mathbf{W}_j^e)$$

the divergence theorem can be readily applied to (4) resulting in the following expression:

$$\begin{aligned} 0 = \sum_{j=1}^{6} E_j^e \Bigg\{ & \int_{V_e} \left(\frac{1}{\mu_r} (\nabla \times \mathbf{W}_i^e) \,.\, (\nabla \times \mathbf{W}_j^e) - k_o^2 \epsilon_r \mathbf{W}_i^e . \mathbf{W}_j^e \right) dv \\ & + \oint_{S_e} \left(\frac{1}{\mu_r} (\nabla \times \mathbf{W}_j^e) \times \mathbf{W}_i^e \right) . \mathbf{dS} \Bigg\} \end{aligned} \qquad (5)$$

where S_e denotes the surface enclosing V_e. Using vector identities , (5) can be further simplified to yield the weak form of Maxwell's equation:

$$\sum_{j=1}^{6} E_j^e \int_{V_e} \left(\frac{1}{\mu_r} (\nabla \times \mathbf{W}_i^e) \,.\, (\nabla \times \mathbf{W}_j^e) - k_o^2 \epsilon_r \mathbf{W}_i^e . \mathbf{W}_j^e \right) dv = \jmath \omega \mu_o \oint_{S_e} \mathbf{W}_i^e . (\mathrm{n} \times \mathbf{H}) ds \qquad (6)$$

where $\mathbf{n} \times \mathbf{H}$ is the tangential magnetic field on the exterior dielectric surface. Equation (6) can be conveniently written in matrix form as

$$[A^e]\,[E^e] = [B^e] \qquad (7)$$

where

$$A_{ij}^e = \int_{V_e} \left(\frac{1}{\mu_r} (\nabla \times \mathbf{W}_i^e) \,.\, (\nabla \times \mathbf{W}_j^e) - k_o^2 \epsilon_r \mathbf{W}_i^e . \mathbf{W}_j^e \right) dv \qquad (8)$$

$$B_i^e = \jmath \omega \mu_o \oint_{S_e} \mathbf{W}_i^e . (\mathrm{n} \times \mathbf{H}) ds \qquad (9)$$

On assembling all the M tetrahedral elements that make up the geometry, we obtain a system of equations whose solution yields the field components over the entire body. Therefore, summing over all M elements, we have

$$\sum_{e=1}^{M}[A^e][E^e] = \sum_{e=1}^{M}[B^e] \tag{10}$$

which gives

$$[A][E] = [B] \tag{11}$$

where $[A]$ is a $N \times N$ matrix with N being the total number of edges resulting from the subdivision of the body and $[E]$ is a $N \times 1$ column vector denoting the edge fields. Due to the continuity of the tangential component of the magnetic field at the interface between two dielectrics, an element face lying inside the body does not contribute to $[B]$ since the surface integrals over the faces of adjacent tetrahedra cancel each other. As a result, $[B]$ is a column vector containing the tangential magnetic field only over the exterior surface of the body. Equation (11) can therefore be written as

$$\begin{aligned} A_{ss}\mathbf{E}_s + A_{si}\mathbf{E}_i &= \mathbf{H}_s \\ A_{is}\mathbf{E}_s + A_{ii}\mathbf{E}_i &= 0 \end{aligned} \tag{12}$$

where the subscript s denotes the edges on the surface and i represents the edges inside the body. It is thus readily seen that (11) relates the electric field inside and on the surface of the body to the on-surface tangential magnetic field.

2 Basis functions

Vector fields within tetrahedral domains in three dimensional space can be conveniently represented by expansion functions that are linear in the spatial variables and have either zero divergence or zero curl. The basis functions defined below are associated with the six edges of the tetrahedron and have zero divergence and constant curl. Assuming the four nodes and the six edges of a tetrahedron are numbered according to Table 1, the vector basis functions associated with the $(7-i)$th edge of the tetrahedron are defined as

$$\mathbf{W}_{7-i} = \begin{cases} \mathbf{f}_{7-i} + \mathbf{g}_{7-i} \times \mathbf{r}, & \mathbf{r} \text{ in the tetrahedron} \\ 0, & \text{otherwise} \end{cases} \tag{13}$$

where $i = 1, 2, \cdots, 6$ and $\mathbf{f}$ and $\mathbf{g}$ are constant vectors. On direct evaluation, it is readily seen that

$$\nabla \cdot \mathbf{W}_i = 0 \quad (14)$$

$$\nabla \times \mathbf{W}_i = 2\mathbf{g}_i \quad (15)$$

Since the complex scalar E_j in (2) is the projection of the electric field onto the jth edge of the tetrahedral element,

$$\mathbf{W}_i \cdot \mathbf{e}_j|_{\mathbf{r}\ on\ jth\ edge} = \delta_{ij} \quad (16)$$

where δ_{ij} is the Kronecker delta. Solving (13) and (16) for the unknown vectors yield[1]

$$\mathbf{f}_{7-i} = \frac{b_{7-i}}{6V}\mathbf{r}_{i_1} \times \mathbf{r}_{i_2} \quad (17)$$

$$\mathbf{g}_{7-i} = \frac{b_i b_{7-i} \mathbf{e}_i}{6V} \quad (18)$$

where V is the volume of the tetrahedral element, $\mathbf{e}_i = (\mathbf{r}_{i_2} - \mathbf{r}_{i_1})/b_i$ is the unit vector of the ith edge and $b_i = |\mathbf{r}_{i_2} - \mathbf{r}_{i_1}|$ is the length of the ith edge. All distances are measured with respect to the origin.
Since there are two numbering systems, local and global, a unique global direction is defined (e.g., always pointing from the smaller node number to the larger node number) to ensure the continuity of $\mathbf{n} \times \mathbf{E}$ across all edges. This implies that (13) should be multiplied by (-1) if the local edge vector (as defined in Table 1) does not have the same direction as the global edge direction. Even though $\mathbf{W}_i$ forces no conditions on the normal component of $\mathbf{E}$, it has been shown[2] that the continuity of electric flux can be satisfied within the degree of approximation with the above formulation. Finally, since $\nabla \cdot \mathbf{W}_i = 0$ the electric field obtained through (2) exactly satisfies the divergence equation within the element, i.e. $\nabla \cdot \mathbf{E} = 0$. Therefore, the finite element solution is free from contamination of spurious solutions[2].

3 Mesh termination

Differential equation methods, such as finite elements, can only solve boundary value problems. Since electromagnetic problems are open boundary-infinite domain types, a means to truncate the solution domain to lie within a finite boundary must be found. On this boundary, a condition is enforced thus ensuring that the fields will obey the Sommerfeld

radiation condition at distances asymptotically far from the object. These absorbing boundary conditions (ABCs) have a significant advantage over the global methods of solving unbounded problems using finite elements in that they are local in nature. Due to this, the sparse matrix structure of the finite element formulation is retained. One disadvantage, however, is that ABCs are approximate and do not model the exterior field exactly. The objective of absorbing boundary conditions is to truncate the finite element mesh with boundary conditions that cause minimum reflections of an outgoing wave. These ABCs should provide small, acceptable errors while minimising the distance from the object of interest to the outer boundary. This minimal distance is required to reduce the number of unknowns in the problem for computational efficiency. A three dimensional vector boundary condition will be investigated here for terminating the finite element mesh of the body described in section 1.1. We begin with the Wilcox representation[3] of the electric field which has an expansion

$$\mathbf{E}(\mathbf{r}) = \frac{e^{-jkr}}{r} \sum_{n=0}^{\infty} \frac{\mathbf{A}_n(\theta, \phi)}{r^n} \tag{19}$$

From (19), we get

$$\nabla \times \mathbf{E} = \left\{ jk\hat{r} \times \frac{1 + D_1}{r} \right\} \mathbf{E} - \frac{e^{-jkr}}{r^2} \sum_{n=1}^{\infty} \frac{n\mathbf{A}_{nt}}{r^n} \tag{20}$$

where $\mathbf{A}_{nt} = \hat{r} \times \mathbf{A}_n$ is the transverse component of $\mathbf{A}_n$ and, for a vector $\mathbf{F}$, $D_1\mathbf{F}$ is given by

$$\begin{aligned} D_1\mathbf{F} &= \frac{1}{sin\theta} \left[\frac{\partial}{\partial\theta}(sin\theta F^{\phi}) - \frac{\partial F^{\theta}}{\partial\phi} \right] \hat{r} \\ &\quad + \frac{1}{sin\theta} \left[\frac{\partial F^{r}}{\partial\theta} - sin\theta F^{\phi} \right] \hat{\theta} + \left[F^{\theta} - \frac{\partial F^{r}}{\partial\theta} \right] \hat{\phi} \end{aligned} \tag{21}$$

Using the recursion relation

$$-2jkn\mathbf{A}_{nt} = n(n-1)\mathbf{A}_{n-1,t} + D_4\mathbf{A}_{n-1}$$

where

$$
\begin{aligned}
D_4\mathbf{A}_n &= \left(D\ A_n^\theta + D_\theta\ \mathbf{A}_n\right)\hat{\theta} + \left(D\ A_n^\phi + D_\phi\ \mathbf{A}_n\right)\hat{\phi} \\
D_\theta\ \mathbf{A}_n &= 2\frac{\partial A_n^r}{\partial\theta} - \frac{1}{sin^2\theta}A_n^\theta - \frac{2cos\theta}{sin^2\theta}\frac{\partial A_n^\phi}{\partial\theta} \\
D_\phi\ \mathbf{A}_n &= \frac{2}{sin\theta}\frac{\partial A_n^r}{\partial\phi} - \frac{1}{sin^2\theta}A_n^\phi + \frac{2cos\theta}{sin^2\theta}\frac{\partial A_n^\theta}{\partial\phi}
\end{aligned}
$$

and D is Beltrami's operator[3], we can derive the representation correct to r^{-4}. Applying the recursion relation in (20) yields the desired relationship for the vector ABC:

$$\nabla \times \mathbf{E} = \alpha(r)\mathbf{E} + \beta(r)D_4\mathbf{E} \tag{22}$$

where

$$\alpha(r) = jk\left\{\frac{D_1}{jkr} - \left(1 + \frac{1}{jkr}\right)\hat{r}\times\right\} \tag{23}$$

$$\beta(r) = \frac{1}{2jkr^2}\frac{1}{(1 + 1/jkr)} \tag{24}$$

The ABC formulated above is applicable to spherical boundaries and hence would be storage intensive and numerically inefficient when used to terminate the mesh of long and thin geometries. It would be highly desirable to choose an outer boundary that conforms to the shape of the object. An approximate boundary condition based on the asymptotic representation of fields for a two dimensional scalar problem has already been derived[4]. It is the author's intention to extend the derivation of the two dimensional scalar boundary condition to a three dimensional vector absorbing boundary condition for an arbitrary outer boundary.

4 Solution of the finite element equations

An inspection of (11) reveals that for an inhomogeneous body, there is no a priori information about the tangential magnetic field over the exterior surface of the body. Relation (11) therefore contains two unknown vectors, $[E]$ and $[B]$, and thus another condition is required involving the two variables to permit an evaluation of the fields inside and on the surface of the body. This condition relating the tangential electric field to the tangential magnetic field on the surface is provided by (22). Since the ABC in (22) refers to the scattered field, we can rewrite it as

$$\begin{aligned} \nabla \times \mathbf{E}_s^s &= \alpha(r)\mathbf{E}_s^s + \beta(r)D_4\mathbf{E}_s^s \\ \mathbf{H}_s^s &= \frac{j}{\omega\mu}\left[\alpha(r)\mathbf{E}_s^s + \beta(r)D_4\mathbf{E}_s^s\right] \\ &= \mathcal{K}\mathbf{E}_s^s \end{aligned} \tag{25}$$

where $\mathcal{K} = \frac{j}{\omega\mu}\left[\alpha(r) + \beta(r)D_4\right]$ and the subscript s denotes the field on the surface and the superscript s represents the scattered field. Since the total field is a sum of the incident field and the scattered field, therefore from (25), we obtain

$$\begin{aligned} \mathbf{H}_s^s &= \mathcal{K}\mathbf{E}_s^s \\ \mathbf{H}_s - \mathbf{H}_s^{inc} &= \mathcal{K}\left(\mathbf{E}_s - \mathbf{E}_s^{inc}\right) \end{aligned} \tag{26}$$

Substituting (26) into (12) and simplifying gives

$$\begin{aligned} (A_{ss} - \mathcal{K})\mathbf{E}_s + A_{si}\mathbf{E}_i &= \mathbf{H}_s^{inc} - \mathcal{K}\mathbf{E}_s^{inc} \\ A_{is}\mathbf{E}_s + A_{ii}\mathbf{E}_i &= 0 \end{aligned} \tag{27}$$

The above equation can thus be solved for the unknown electric fields both inside and on the surface of the body.

5 References for Appendix A

1. M.L. Barton and Z.J. Cendes, "New vector finite elements for three-dimensional magnetic field computation", *J. Appl. Phys.*, vol.61, no.8, pp.3919-21, April 1987.

2. X. Yuan, "On the use of divergenceless basis functions in finite elements", submitted to *Electron. Lett.*

3. C.H. Wilcox, "An expansion theorem for electromagnetic fields", *Comm. Pure Appl. Math.*, vol. 9, pp. 115-134, May 1956.

4. A. Khebir, O.M. Ramahi and R. Mittra, "An efficient partial differential equation method to solve complex shape scatterers", to appear.

TABLE I

TETRAHEDRON EDGE DEFINITION

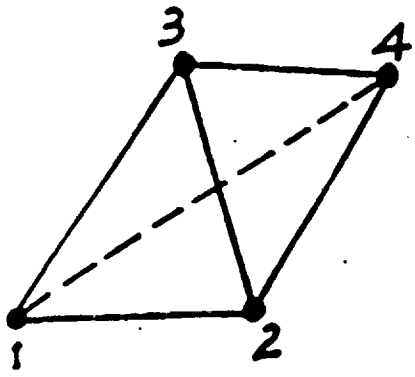

Edge #	i_1	i_2
1	1	2
2	1	3
3	1	4
4	2	3
5	4	2
6	3	4